JBIC (1998) 3:150–160 © SBIC 1998

ORIGINAL ARTICLE

Gerard J. Colpas · Timothy G. Brayman
John McCracken · Michelle A. Pressler
Gerald T. Babcock · Li-June Ming
Christopher M. Colangelo · Robert A. Scott
Robert P. Hausinger

Spectroscopic characterization of metal binding by *Klebsiella aerogenes* UreE urease accessory protein

Received: 8 October 1997 / Accepted: 30 December 1997

Abstract The urease accessory protein encoded by *ureE* from *Klebsiella aerogenes* is proposed to function in Ni(II) delivery to the urease apoprotein. Wild-type UreE contains a histidine-rich region at its carboxyl terminus and binds 5–6 Ni per dimer, whereas the functionally active but truncated H144*UreE lacks the histidine-rich motif and binds only two Ni per dimer [Brayman TG, Hausinger RP (1996) J Bacteriol 178:5410-5416]. For both proteins, Cu(II), Co(II), and Zn(II) ions compete for the Ni-binding sites. In order to characterize the coordination environments of bound metals, especially features that are unique to Ni, the Ni-, Cu-, and Co-bound forms of H144*UreE were studied by a combination of EPR, ESEEM, hyperfine-shifted ^{1}H-NMR, XAS, and RR spectroscopic methods. For each metal ion, the two binding sites per homodimer were spectroscopically distinguishable. For example, the two Ni-binding sites each have pseudo-octahedral geometry in an N/O coordination environment, but differ in their number of histidine donors. The two Cu-binding sites have tetragonal geometry with two histidine donors each; however, the second Cu ion is bound by at least one cysteine donor in addition to the N/O-type donors found for the first Cu ion. Two Co ions are bound to H144*UreE in pseudo-octahedral geometry with N/O coordination, but the sites differ in the number of histidine donors that can be observed by NMR. The differences in coordination for each type of metal ion are relevant to the proposed function of UreE to selectively facilitate Ni insertion into urease in vivo.

Key words Urease · Nickel · UreE · Accessory protein · Spectroscopy

Abbreviations *EPR* electron paramagnetic resonance · *ESEEM* electron spin echo envelope modulation · *NMR* nuclear magnetic resonance · *XAS* X-ray absorption spectroscopy · *EXAFS* extended X-ray absorption fine structure · *RR* resonance Raman · *FT* Fourier transform

Introduction

Urease (EC 3.5.1.5) is a Ni-dependent enzyme that catalyzes the hydrolysis of urea to form ammonia and carbamate [1]. *Klebsiella aerogenes* urease has been structurally characterized [2] and shown to contain a dinuclear Ni-active site located in a tightly associated trimer of three subunits [i.e., $(\alpha\beta\gamma)_3$ stoichiometry] encoded by *ureA*, *ureB*, and *ureC*. In vivo activation of this enzyme requires the participation of four accessory proteins encoded by genes (*ureD*, *ureE*, *ureF*, and *ureG*) found adjacent to the enzyme structural genes [3].While deletions within *ureD*, *ureF*, or *ureG* lead to the production of inactive urease in vivo, a deletion within *ureE* only reduces the specific activity of the purified urease by approximately half. The specific roles of the UreD, UreF, and UreG proteins are not understood [4]; however, they are known to form a series of complexes with urease apoprotein [5–7]. In contrast,

G. J. Colpas · T. G. Brayman · R. P. Hausinger (✉)
Departments of Microbiology and Biochemistry, Michigan State University, East Lansing, MI 48824-1101, USA
Tel.: +1-517-353-9675; Fax: +1-517-353-8957;
e-mail: hausinge@pilot.msu.edu

J. McCracken · M. A. Pressler · G. T. Babcock
Department of Chemistry, Michigan State University, East Lansing, MI 48824, USA

L.-J. Ming
Department of Chemistry and Institute for Biomolecular Science, University of South Florida, Tampa, FL 33620-5250, USA

C. M. Colangelo · R. A. Scott
Center for Metalloenzyme Studies, Departments of Chemistry and Biochemistry & Molecular Biology, University of Georgia, Athens, GA 30602-2556, USA

Supplementary material Table 1 of additional fits for Ni and Cu EXAFS of H144*UreE has been deposited in electronic form and can be obtained from http://link.springer.de/linkservice/journals/00775

UreE, the focus of this manuscript, does not appear to complex with urease; rather, it has been proposed to function in delivery of Ni ions to urease apoprotein [8].

Purified *K. aerogenes* UreE reversibly binds 5–6 Ni(II) ions per homodimer (average $K_d \approx 10\ \mu M$) [8]. Results of X-ray absorption spectroscopy (XAS) and variable-temperature magnetic circular dichroism spectroscopy experiments with this protein indicate the presence of pseudo-octahedral Ni(II) coordinated by an average of 3–5 imidazole ligands [8]. The apparent requirement for 15–30 histidines per dimer for binding Ni implicates a role for the carboxyl terminus, where 10 of the last 15 residues are histidine. Despite its distinctive sequence, however, the histidine-rich region found in *K. aerogenes* protein is not conserved in all UreE homologs [4].

A truncated form of UreE, termed H144*UreE, has been isolated from *Escherichia coli* cells containing the *K. aerogenes* urease gene cluster with a *ureE* mutation that causes translational termination at a position corresponding to the 15th residue from the normal carboxyl terminus [9]. In vivo studies with cells producing H144*UreE demonstrate that internal Ni-binding sites, not the histidines at the carboxyl terminus, are necessary for this protein to assist in *K. aerogenes* urease activation [9]. Equilibrium dialysis measurements with H144*UreE indicate that two Ni(II) per dimer are cooperatively bound, with half-saturation at $\sim 10\ \mu M$ of this metal ion. Competition experiments with Cu, Zn, Co, and Cd indicate that these divalent metal ions compete (to varying degrees) with Ni binding to H144*UreE in vitro, raising questions about the potential ability of these metals to compete in vivo [9].

We have chosen to further study Ni, Cu, and Co binding to H144*UreE by using an array of spectroscopic techniques. For each metal ion, the two binding sites per homodimer are found to be spectroscopically distinct. In addition, the coordination environments are shown to differ for each type of metal. The ability of UreE to function selectively as a Ni donor to urease is discussed in terms of the observed distinct binding mode for Ni as compared to that of other transition metals.

Materials and methods

Purification of protein

Genes encoding wild-type and H144*UreE were over-expressed in *E. coli* HMS174 (DE3) cells carrying the pET21 plasmid derivatives pETWT or pETH144* (cells and vector from Novagen, Madison, Wis.), and proteins were purified and concentrated as previously described [9]. Protein concentrations were measured using a commercial assay (Bio-Rad) with bovine serum albumin as the standard. For cysteine modification experiments, a sample of H144*UreE in 100 mM Tris-HCl buffer (pH 7.9) was incubated with 5.0 mM iodoacetamide for one hour at 37 °C and desalted using a Superose-12 column (1 × 30 cm).

Electronic spectroscopy

Electronic absorption spectra were recorded and analyzed on a DU-7500 UV-visible spectrophotometer (Beckman, Fullerton, Calif.). Samples were prepared in 10 mM Tris-HCl buffer (pH 7.5) with 50 mM NaCl (and 15% glycerol for Co), and spectra were recorded in a 1-ml cuvette at room temperature. 20 mM solutions of metal chloride salts in water were titrated into 200 or 600 μM H144*UreE solutions. Background corrections for the cuvettes and buffers were applied.

Electron paramagnetic resonance (EPR) spectra

X-band EPR spectra were obtained on a Bruker ESP–300E spectrometer. Samples were prepared in 10 mM Tris-HCl buffer (pH 7.5) with 50 mM NaCl and 30% glycerol to aid in glass formation. Spectra were recorded in frozen solution at 77 K.

Electron spin echo envelope modulation (ESEEM) spectroscopy

ESEEM data were collected at X-band on a homebuilt spectrometer described elsewhere [10]. Data were collected using a standard stimulated echo pulse sequence. ESEEM spectra were obtained by Fourier transformation of the envelope decay functions using a dead-time reconstruction method [11]. Samples were dissolved in 10 mM Tris-HCl buffer (pH 7.5) with 50 mM NaCl and 30% glycerol to aid in glass formation, and recorded in frozen solution at 4 K.

Hyperfine-shifted ^{1}H nuclear magnetic resonance (NMR) studies

The proton NMR spectra of the paramagnetic Ni(II) and Co(II) derivatives of H144*UreE were acquired at 298 K on a Bruker AMX360 NMR spectrometer operated at 360 MHz. A single 90-deg pulse with a 50 to 100 ms presaturation decoupler pulse was used to obtain spectra. A Gaussian apodization function with a 5% shift and a line-broadening factor of –50 Hz was applied to the FIDs prior to Fourier transformation. Selective excitation of solvent exchangeable signals was performed using the 1-*3*–3-*1* hard pulse sequence [12]. Samples were prepared in 10 mM phosphate buffer (pH 7.2) with 10% D_2O added to use as a frequency lock. To determine the solvent exchangeability of protons, samples were prepared in 90% D_2O buffer (100% D_2O buffer led to protein precipitation).

X-ray absorption spectroscopy (XAS)

Samples of 1.1 mM H144*UreE were titrated with 1 or 2 equivalents of metal chloride solutions in 10 mM Tris-HCl buffer (pH 7.5) with 30% glycerol to aid in glass formation. XAS data collection was performed at the Stanford Synchrotron Radiation Laboratory (SSRL) with SPEAR operating at 3.0 GeV, 50–100 mA by previously described methods [13]. Details of the data collection and reduction are summarized in Table 1. Standard EXAFS analysis was performed [13] using EXAFSPAK software (http://ssrl01.slac.stanford.edu/exafspak.html). Both single and multiple-scattering paths 4.5 Å from either the Cu or Ni atom were used to identify and quantify imidazole coordination due to histidine. Multiple-scattering paths were built by taking the crystal structure of tetrakis (imidazole) copper(II) sulfate [14] or hexakis (imidazole) nickel(II) chloride tetrahydrate [15] and importing it into Ball & Stick software (v. 3.5, Cherwell Scientific). The model was edited to only the metal atom and one imidazole and the coordinates were then imported into FEFF v. 5.05 software [16–18] to calculate scattering amplitudes and phase shifts for each scattering path containing four or fewer legs. A constrained fitting process was then used with the following parameters.

Table 1 X-ray absorption spectroscopic data collection and reduction for *Klebsiella aerogenes* H144*UreE

Element	Ni	Cu
SR facility	SSRL	SSRL
Beamline	7–3	7–3
Monochromator crystal	Si[220]	Si[220]
Detection method	Fluorescence	Fluorescence
Detector type	Solid state array[a]	Solid state array[a]
Scan length, min	28	27
Scans in average	8 (2 Ni), 16 (1 Ni)	10 (2 Cu), 12 (1 Cu)
Temperature, K	10	10
Energy standard	Ni foil (first inflection)	Cu foil (first inflection)
Energy calibration, eV	8331.1	8980.3
E_0, eV	8340	8990
Pre-edge background		
Energy range, eV	8005–8295	8650–8945
Gaussian center, eV	7390	8040
Width, eV	900 (2 Ni), 1125 (1 Ni)	1100
Spline background		
Energy range, eV	8340–8574 (4)	8990–9210 (4)
(polynomial order)	8574–8809 (4)	9210–9430 (4)
	8809–9043 (3)	9430–9650 (3)

[a] The 13-element Ge solid-state X-ray fluorescence detector at SSRL is provided by the NIH Biotechnology Research Resource

Coordination numbers were constrained to be integer values. The distances and Debye-Waller factors for outer-shell atoms of imidazole rings were constrained to a given ratio with first shell (metal-nitrogen/oxygen) distance and Debye-Waller factor, respectively. In many fits, the first coordination sphere contains imidazole nitrogens plus additional non-imidazole (N,O)-containing ligands. Separating these into two shells with independent M-(N,O) distances had no more than a small effect on the fits. If the separation improved the goodness-of-fit statistic then these fits are reported. If not, fits in which a single M-(N,O) distance was used for both imidazole and non-imidazole ligands are reported. First-shell distances are expected to be accurate to within ± 0.02 Å. The bond valence sum method was applied to EXAFS fits using standard procedures [19–21].

Resonance Raman (RR) studies

Spectra were obtained using a SPEX 1401 spectrometer equipped with a photon-counting photomultipier detector. Excitation at 413.1 nm was provided by a krypton ion laser (Coherent Innova 90). Sample was dissolved in 10 mM HEPES buffer (pH 7.5) with 50 mM NaCl and 30% glycerol. A control buffer solution was examined under identical conditions. Both control and protein sample spectra were obtained in capillary sample cells at 13.5 mW and maintained at 4 °C with a stream of cold N_2 gas.

Results

An array of spectroscopic methods was used to examine Ni, Cu, and Co binding by H144*UreE, a truncated *K. aerogenes* UreE protein that retains nearly complete in vivo function in assisting urease dinuclear Ni assembly. In selected cases, comparative data were obtained for the full length protein in order to confirm the relevance of the results obtained on the truncated form. It is important to note that equilibrium dialysis studies have shown that Ni binding to H144*UreE is cooperative [9] (i.e., the addition of one equivalent of Ni per dimer results in protein forms containing 2Ni/dimer and 0Ni/dimer, as well as 1Ni/dimer). Analysis of previously published Ni-binding data [9] yields a Hill coefficient of 1.69 consistent with positive cooperativity. Cu binding has also been suggested to exhibit cooperativity [9], while nothing is known about Co-binding cooperativity.

Electronic spectroscopy

UV-visible spectra were recorded for samples of H144*UreE that were titrated with Ni(II), Cu(II), and Co(II). The Ni titration (Fig. 1a) revealed a weak band at approximately 380 nm ($\varepsilon \approx 75\ M^{-1}\ cm^{-1}$) that was approximately half developed with one equivalent and fully developed upon addition of two equivalents of Ni to the dimer. In agreement with prior results [9], the addition of Cu to H144*UreE (Fig. 1b) led to the development of a sharp band at 370 nm ($\varepsilon \approx 2500\ M^{-1}\ cm^{-1}$), that appeared to be generated primarily with the addition of the second equivalent of Cu to the dimer, and a broad absorbance observed near 625 nm ($\varepsilon \approx 250\ M^{-1}\ cm^{-1}$). The 370-nm band had the intensity characteristic of a charge-transfer transition while the 625 nm band was more consistent with a d-d transition typical of a 5- or 6-coordinate tetragonal Cu(II) site as observed previously in many proteins and complexes [22, 23]. Spectra observed in the presence of Co (Fig. 1c) indicated an increase in absorbance in the visible region upon addition of the first two equivalents of metal due to d-d transitions centered near 500 nm ($\varepsilon \approx 20\ M^{-1}\ cm^{-1}$). The spectra lack evidence of any charge-transfer transitions, and are typical of pseudo-octahedral Co(II) coordinated by N/O donors [24].Visible spectra obtained with wild-type UreE were indistinguishable from those obtained with H144*UreE in all cases (data not shown).

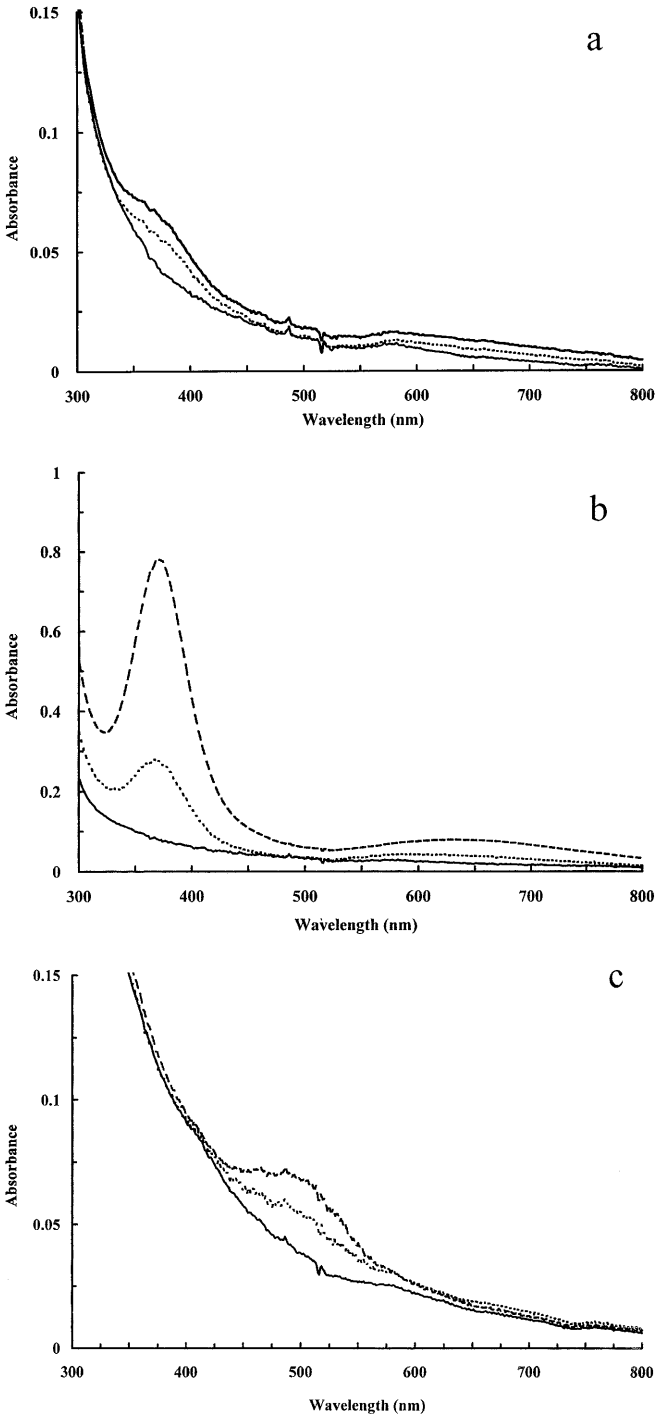

Fig. 1a–c Electronic spectra of H144*UreE titrated with selected metal ions. The spectra shown are for H144*UreE (200 μM dimer for Ni and Cu, and 600 μM dimer for Co) in 10 mM Tris-HCl buffer (pH 7.5) with 50 mM NaCl (and 15% glycerol for Co) in the presence of 0 (*solid line*), 1 (*dotted line*), or 2 (*dashed line*) equivalents of Ni(II) (**a**), Cu(II) (**b**), or Co(II) (**c**)

H144*UreE was incubated with iodoacetamide to modify any exposed cysteine residues prior to titration with Ni or Cu. Titration of the chemically modified protein with Cu failed to produce a 370-nm charge-transfer band, although the 625-nm d-d band was still visible (data not shown). By contrast, no change was observed in the intensity or location of the weak band centered at 380 nm for the alkylated protein titrated with Ni (data not shown).

EPR spectroscopy

Spectra were obtained for H144*UreE in the presence of one or two equivalents of Cu (Fig. 2). Both spectra are typified as tetragonal type 2 Cu sites; however, important but subtle differences were observed between these two spectra. The 1Cu/dimer spectrum yielded g–values of 2.28 and 2.06 with A_z = 158 G arising from Cu hyperfine. Superhyperfine splitting was observed in g_{xy} with ~ 15-G spacing typical of ^{14}N directly bound to the Cu [25]. Addition of the second Cu per dimer resulted in the superimposition of a distinct spectrum (g values of 2.32 and 2.07 with A_z = 155 G) on the first spectrum. The superhyperfine splitting was broadened out and not distinguishable. There was no evidence of coupling between the two Cu(II) ions.

ESEEM spectra

ESEEM data obtained at X-band on the 1Cu/dimer and 2Cu/dimer forms of H144*UreE showed modulation patterns indicative of equatorial histidine ligands. For the 1Cu/dimer H144*UreE sample (Fig. 3a), a characteristic pattern of three sharp lines at 0.55, 1.0 and 1.55 MHz, and a broad peak centered at 4.1 MHz arose from ligand hyperfine coupling between the metal and remote ^{14}N of bound imidazole(s) [26]. The minor features resolved at 2.1, 2.6 and 3.1 MHz are combination features of the sharp low-frequency lines that result from the presence of a second ^{14}N coupled to the metal in a nearly identical fashion to the first [27–29]. ESEEM data for the 2Cu/dimer sample were also characterized by deep ^{14}N modulations with the intensities of the modulations showing a slight decrease from those obtained for the 1Cu/dimer sample. To isolate the ESEEM pattern associated with the second Cu site, data from the two samples (containing the same concentration of apo-H144*UreE) were normalized by scaling the amplitude of the 1Cu/dimer ESEEM to be half that of the 2Cu/dimer form at the longer pulse-spacing times ($\tau + T$ = 10.4 msec). At these longer times, the echo modulations have ceased and the amplitudes of the echos reflect the Cu concentration in the sample as long as the two sites are characterized by similar spin-lattice relaxation times. After this scaling was completed, the ESEEM data from the 1Cu/dimer sample was subtracted from that of the 2Cu/dimer sample, and subsequent Fourier transformation gave rise to the spectrum of Fig. 3b. These data show that the second Cu site also features the weak combination lines indicative of at least two equatorially bound histidyl imidazole ligands. The differences between the ESEEM

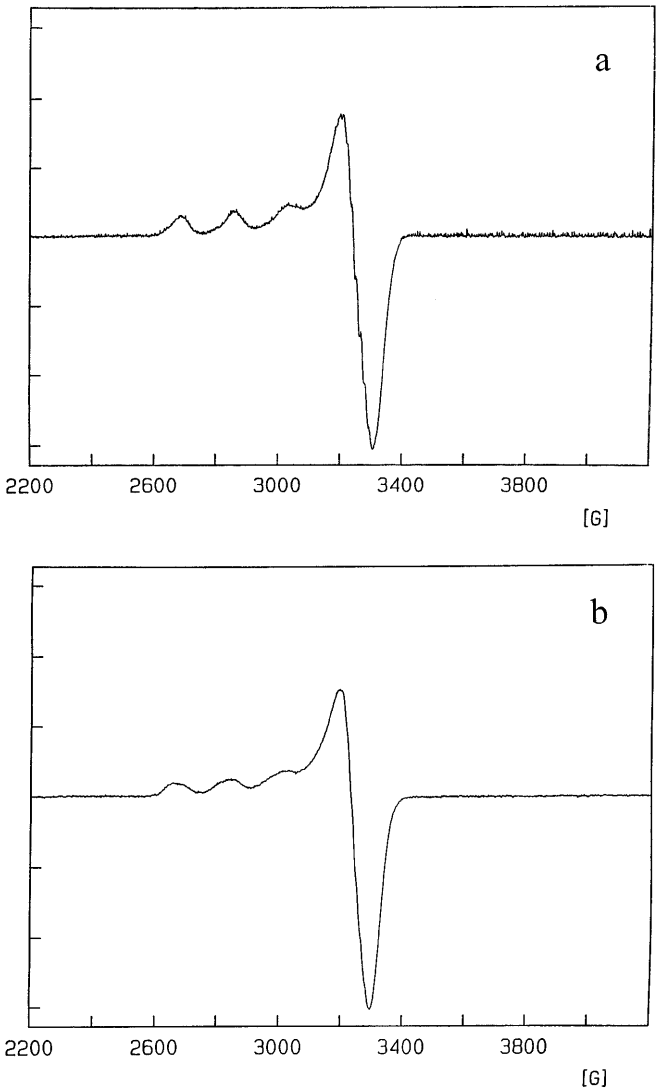

Fig. 2a,b X-band EPR spectra of Cu-H144*UreE. Samples of H144*UreE (0.60 mM dimer) in 10 mM Tris-HCl buffer (pH 7.5) with 50 mM NaCl and 30% glycerol were incubated with one (**a**) or two (**b**) equivalents of Cu. Spectra were obtained in frozen solution at 77 K

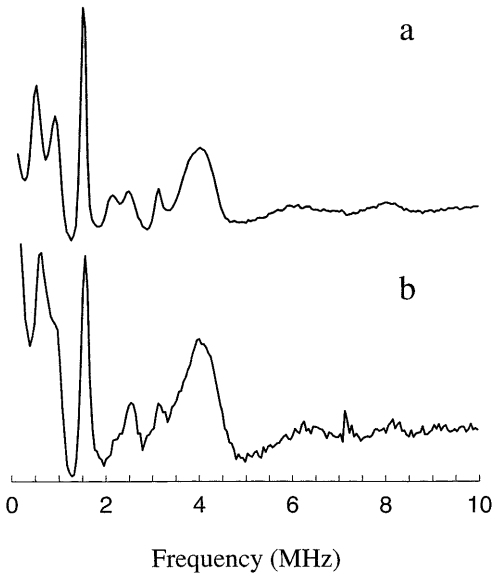

Fig. 3 ESEEM spectra of Cu-H144*UreE. Spectra represent the 1Cu/dimer (*a*) and the second Cu-site (*b*) of the 2Cu/dimer species. Spectra were obtained by Fourier transformation of the time domain ESEEM data using dead-time reconstruction. For spectrum *a*, the data were processed directly. For *b*, the data set of *a* was normalized so that its amplitude at $\tau+T$ at 10.4 msec was equal to half that of the 2Cu/dimer sample collected under identical conditions and the difference of the two time domain data sets was subjected to Fourier analysis. Conditions common to both measurements were: microwave frequency 9.00 GHz, field strength 3100 G, τ 360 ns; microwave power 50 W (20 ns FWHM pulses), sample temperature 4.2 K, pulse repetition rate 60 Hz; H144*UreE concentration 1.0 mM, and 34 events were averaged per ESEEM trace

spectra of the two Cu sites reflect small differences in the asymmetry parameter of the ^{14}N nuclear quadrupole interaction. The difference observed here is subtle and may be attributable to differences in solvent accessibilty to the remote histidyl nitrogens [30].

Hyperfine-shifted ^{1}H NMR

Titrations of H144*UreE with Ni(II) and Co(II) ions were followed by ^{1}H NMR. In the case of Ni (Fig. 4a), one broad and three sharp resonances were observed in the paramagnetically shifted region between 60 and 75 ppm. The 1Ni/dimer sample exhibited a sharp resonance at 62.6 ppm and two smaller features at 65.3 and 73.0 ppm. The latter two resonances grew into sharp peaks in the 2Ni/dimer sample. No additional signals were detected by the use of a selective excitation 1-*3*–3-*1* hard pulse sequence. All three sharp resonances disappeared in the spectrum of a sample in 90% D_2O. The broad resonance occurring in this region of the spectrum was not eliminated by solvent exchange, and likely arises from imidazole ring CH protons. There was no evidence of additional signals due to other ligands in the spectrum of the Ni(II)-treated sample, although several peaks were observed between 20 and 35 ppm after the second equivalent of Ni was added.

The addition of Co(II) to H144*UreE led to the appearance of two sharp resonances at 63.1 and 76.3 ppm (Fig. 4b). The intensity of these signals was significantly decreased when a presaturation pulse was used for water suppression, consistent with these signals being solvent exchangeable. Spectra from 1Co/dimer and 2Co/dimer samples exhibited little change of line shape, but exhibited an increase in intensity of both signals, particularly the 76.3-ppm resonance, with increasing Co. The signals integrated to yield ratios of $\sim$ 1:1 for the 1Co/dimer sample and $\sim$ 1:2 for the 2Co/dimer sample when the spectra were acquired with a selective excitation pulse (inset Fig. 4b). Two unidentified paramagnetically shifted resonances also were apparent at approximately 15 ppm.

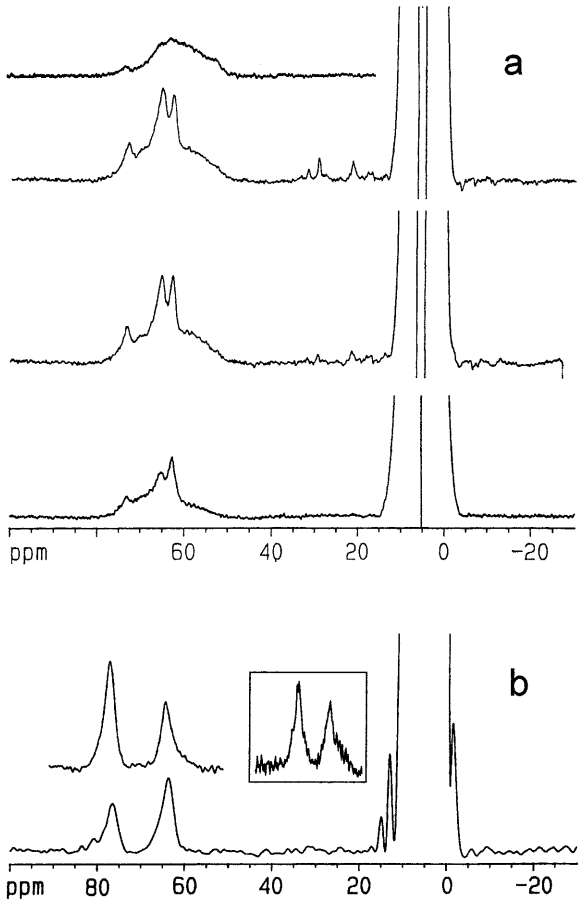

Fig. 4a,b Hyperfine-shifted ^{1}H NMR spectra of H144*UreE with bound Ni and Co. Protein (1.0 mM) in H_2O buffer was examined at 360 MHz and 298 K with 1, 2, and 3 equivalents Ni(II) per dimer (**a**, *bottom* to *top*) and 2 equivalents Co(II) per dimer (**b**) acquired with a 90 deg pulse and a presaturation decoupler pulse for water suppression. The inset in **a** is the spectrum for 2Ni/dimer in D_2O, while the inset in **b** is the spectrum for 2Co/dimer sample acquired with a 1-*3*-3-*1* selective excitation hard-pulse sequence eliminating solvent exchange complications and allowing integration of the signals. The boxed inset in **b** is the spectrum for 1Co/dimer sample acquired with the selective hard-pulse sequence and normalized to the intensity of the 63.1-ppm signal of the 2Co/dimer sample

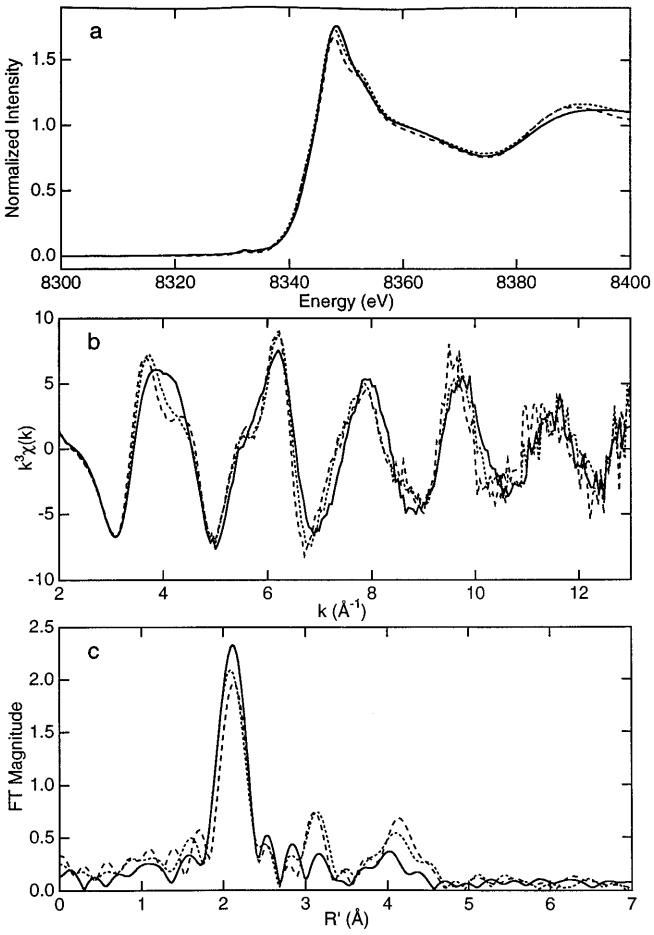

Fig. 5a–c Ni K-edge XAS data of Ni bound to H144*UreE. The normalized edge region (**a**), EXAFS data (**b**), and Fourier transform (**c**) for 1Ni/dimer (*short dashes*) and 2Ni/dimer (*solid line*) are compared to data from wild-type UreE containing ~ 3Ni/dimer (*long dashes*). Samples contained 1.1 mM dimer in 10 mM Tris-HCl buffer (pH 7.5) and 30% glycerol. Spectra were obtained in frozen solution at 10 K

XAS

Samples of H144*UreE with 1Ni/dimer and 2Ni/dimer were analyzed by XAS and compared to data previously obtained for the wild-type UreE dimer sample with approximately three Ni ions bound [8] (Fig. 5). The edge data obtained for the H144*UreE samples were very similar to that for wild-type UreE, and are consistent with octahedral Ni [31]. While the EXAFS regions and Fourier transforms of spectra for 1Ni/dimer sample of H144*UreE also closely resembled that for wild-type protein, the Fourier transform of 2Ni/dimer sample displayed significant decreases in the second and third shell FT peaks associated with histidine ligation (Fig. 5c). Curve-fitting of the Ni EXAFS was most consistent with 6- or 7-coordination including 3–4 histidine donors for the 1Ni/dimer sample and similar coordination with 2–3 histidine donors for the 2Ni/dimer sample (Table 2, additional fits are available as supplementary material). Bond valence sums [19–21] were all near 2.0 for 6- or 7-coordinate fits, as expected for a Ni(II) site (Table 2). For the 2Ni/dimer case, inclusion of 0.5 Ni-S interactions (i.e., S coordination to one Ni) slightly improved the fit; however, the minimal extent of this improvement did not provide clear evidence for the presence of a sulfur ligand.

H144*UreE samples containing one and two equivalents of Cu exhibited XAS edge data that were quite similar to each other indicating a nearly identical coordination geometry in each, but differences were observed in the analysis of the EXAFS (Fig. 6). EXAFS of the 1Cu/dimer and 2Cu/dimer were best fit (Table 3 and supplementary material) by assigning four-coordination including approximately two histidine donors. These four ligands are expected to be the equatorial ligands of a distorted tetragonal site, and the bond val-

Table 2 Curve-fitting results for Ni EXAFS of H144* UreE[a]

Sample	Fit	Group	Shell	N_s	R_{as} (Å)	σ^2_{as} (Å^2)	ΔE_0 (eV)	f' [b]	BVS[f]
Truncated UreE,	1	imid + N/O	Ni-N	(6)[d]	2.08	0.0030	1.37	0.074	1.86
1 Ni/dimer		imid	Ni-C_2	(3)	[3.04][e]	0.0021	[1.37]	<0.056>[c]	
k = 2.0–13.0 Å^{-1}		imid	Ni-N_3	(3)	[4.17]	[0.0029]	[1.37]		
		imid	Ni-C_4	(3)	[4.23]	[0.0029]	[1.37]		
		imid	Ni-C_5	(3)	[3.11]	[0.0021]	[1.37]		
	2	imid + N/O	Ni-N	(6)	2.08	0.0030	1.46	0.074	1.86
		imid	Ni-C_2	(4)	[3.04]	0.0035	[1.46]	<0.057>	
		imid	Ni-N_3	(4)	[4.17]	[0.0049]	[1.46]		
		imid	Ni-C_4	(4)	[4.22]	[0.0049]	[1.46]		
		imid	Ni-C_5	(4)	[3.11]	[0.0036]	[1.46]		
	3	imid + N/O	Ni-N	(7)	2.08	0.0039	1.40	0.068	2.17
		imid	Ni-C_2	(4)	[3.04]	0.0035	[1.40]	<0.051>	
		imid	Ni-N_3	(4)	[4.17]	[0.0049]	[1.40]		
		imid	Ni-C_4	(4)	[4.23]	[0.0049]	[1.40]		
		imid	Ni-C_5	(4)	[3.11]	[0.0036]	[1.40]		
Truncated UreE	4	N/O	Ni-N	(4)	2.05	0.0028	3.87	0.075	1.92
2 Ni/dimer		imid	Ni-N_1	(2)	2.11	0.0010	[3.87]	<0.063>	
k = 2.0–13.5 A^{-1}		imid	Ni-C_2	(2)	[3.08]	[0.0015]	[3.87]		
		imid	Ni-N_3	(2)	[4.23]	[0.0021]	[3.87]		
		imid	Ni-C_4	(2)	[4.28]	[0.0021]	[3.87]		
		imid	Ni-C_5	(2)	[3.15]	[0.0016]	[3.87]		
	5	N/O	Ni-N	(3)	2.05	0.0024	3.56	0.077	1.89
		imid	Ni-N_1	(3)	2.10	0.0023	[3.56]	<0.066>	
		imid	Ni-C_2	(3)	[3.06]	[0.0034]	[3.56]		
		imid	Ni-N_3	(3)	[4.21]	[0.0047]	[3.56]		
		imid	Ni-C_4	(3)	[4.26]	[0.0047]	[3.56]		
		imid	Ni-C_5	(3)	[3.14]	[0.0035]	[3.56]		
	6	N/O	Ni-N	(4)	2.06	0.0038	3.48	0.069	2.19
		imid	Ni-N_1	(3)	2.10	0.0027	[3.48]	<0.059>	
		imid	Ni-C_2	(3)	[3.06]	[0.0040]	[3.48]		
		imid	Ni-N_3	(3)	[4.20]	[0.0055]	[3.48]		
		imid	Ni-C_4	(3)	[4.25]	[0.0055]	[3.48]		
		imid	Ni-C_5	(3)	[3.14]	[0.0047]	[3.48]		
	7	S	Ni-S	(0.5)	2.25	0.0022	0.79	0.064	2.13
		imid + N/O	Ni-N	(6)	2.07	0.0037	[0.79]	<0.051>	
		imid	Ni-C_2	(2)	[3.01]	0.0049	[0.79]		
		imid	Ni-N_3	(2)	[4.14]	[0.0068]	[0.79]		
		imid	Ni-C_4	(2)	[4.19]	[0.0069]	[0.79]		
		imid	Ni-C_5	(2)	[3.08]	[0.0051]	[0.79]		

[a] Group is the chemical unit defined for the multiple-scattering calculation. N_s is the number of scatterers (or groups) per metal. R_{as} is the metal-scatterer distance. σ^2_{as} is a mean square deviation in R_{as}. ΔE_0 is the shift in E_0 for the theoretical scattering functions

[b] f' is a normalized error (chi-squared):

$$f' = \frac{\left\{ \sum_i [k^3(\chi_i^{obs} - \chi_i^{calc})]^2 / N \right\}^{1/2}}{[(k^3\chi^{obs})_{max} - (k^3\chi^{obs})_{min}]}$$

[c] Numbers in angle brackets are f' for the smoothed data

[d] Numbers in parentheses were not varied during optimization

[e] Numbers in square brackets were constrained to be a multiple of the above value

[f] BVS = $\sum s$, $s = e^{[(r_0 - r)/B]}$, $B = 0.37$, $r_0(Ni^{2+} - S) = 1.937$, $r_0(Ni^{2+} - N) = 1.647$, $r_0(Cu^{2+} - S) = 2.060$, $r_0(Cu^{2+} - N) = 1.751$

ence sum analysis (yielding values near 2.0) supported this coordination. For the 1Cu/dimer sample, addition of a Cu-S interaction improved the fit, but the Debye-Waller factor was quite large (meaning low occupancy or high disorder). For the 2Cu/dimer sample, addition of either 0.5 or 1.0 Cu-S interactions per Cu atom (i.e., one or two Cu-S bonds per protein dimer) at 2.24 Å improved the fit significantly and was supported by a reasonable Debye-Waller factor (e.g., fit 6, Table 3).

Resonance Raman (RR) spectra

The 2Cu/dimer sample of H144*UreE was excited by laser irradiation at 413.1 nm, which is in resonance with the 370-nm charge-transfer band, and analyzed by using RR spectroscopy. The spectrum obtained had three resonance-enhanced peaks (239, 282 and 315 cm^{-1}) located in the low-frequency region of the spectrum (Fig. 7) with the maximum intensity associated with the 315 cm^{-1} band. Peaks at approximately 416 and

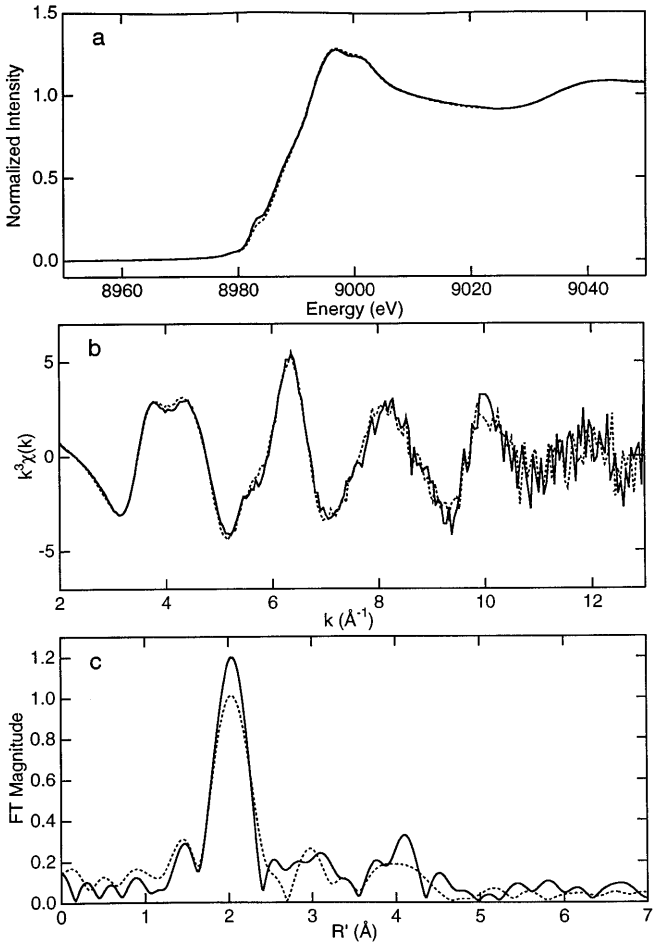

Fig. 6a–c Cu K-edge XAS data of Cu bound to H144*UreE. The normalized edge region (**a**), EXAFS data (**b**), and Fourier transform (**c**) for 1Cu/dimer (*solid line*) and 2Cu/dimer (*dashed line*) are compared. Samples contained 1.1 mM dimer in 10 mM Tris-HCl buffer (pH 7.5) and 30% glycerol. Spectra were obtained in frozen solution at 10 K

487 cm^{-1} were derived from the 30% glycerol needed to keep the protein in solution after addition of Cu.

Discussion

The experiments described above provide insight into how UreE, a urease accessory protein that is capable of binding several different divalent metal ions, may be able to function as a specific Ni donor to urease apoprotein. To simplify our analyses, we chose to study a functionally intact, but truncated, *K. aerogenes* UreE that lacked fifteen residues including ten histidines at the carboxyl terminus. The key findings from these studies include: (1) the two metal ion binding sites in the H144*UreE homodimer are spectroscopically distinguishable, and (2) the coordinating ligands differ for different metal ions. Below, the binding sites for Ni, Cu, and Co are discussed in more detail, and the in vivo implications for functional urease assembly are described.

Ni binding to H144*UreE

The interaction of H144*UreE with Ni was studied by electronic and NMR spectroscopies and by XAS. Prior studies had shown that Ni binding is partially cooperative [9]; hence, protein in the presence of one equivalent of Ni per dimer will include a mixture of protein species containing 2, 1, and 0 Ni ions. The visible spectrum indicates the presence of a d-d band at 380 nm of an intensity that likely arises from 5-coordinate Ni(II) [24, 32, 33]. The intensity of this band nearly doubles when the Ni concentration goes from one equivalent Ni/dimer to 2Ni/dimer, suggesting that the absorbance arises from both Ni-binding sites. The sharp, isotropically-shifted solvent-exchangeable resonances in the proton NMR spectrum can be assigned to coordinated histidine ring NH protons [34]. The intensities of the resonances in the 1Ni/dimer and 2Ni/dimer samples are consistent with partial cooperativity (e.g., the 1Ni/dimer sample mainly possesses the 62.6-ppm resonance, but the two smaller resonances are also present) and suggest the presence of one histidine at the first Ni binding site and two at the second. The slight differences in chemical shift of these histidines arise from subtle differences in their environments. These assignments represent the minimum number of coordinated histidine residues, i.e., additional imidazoles may bind to Ni but not be detected because of the fast solvent exchange of the ring NH protons. The absence of sharp, solvent-non-exchangeable CH signals correlating with these histidine resonances indicates that the Ni(II) coordinates via the N( ) nitrogens. Detection of the broad resonance arising from ring CH protons supports this assignment. NMR provided no clear evidence for the identity of other ligands, although several weak peaks appear (between 20 and 35 ppm) in the presence of excess Ni. These resonances may be attributed to adventitious binding of the metal. X-ray edge and EXAFS spectra are consistent with pseudo-octahedral coordination geometries for both the 1Ni/dimer and 2Ni/dimer forms. The apparent conflict with the coordination geometry indicated by the visible spectrum may simply reflect a function of the temperature at which the spectra were run. Since the EXAFS fits indicated the presence of 3–4 imidazole ligands in the 1Ni/dimer species and 2–3 histidines in the 2Ni/dimer sample, they suggest that either the second Ni was bound to a site with fewer histidines than the first or that ligand exchange between the two sites must exist. The NMR data are compatible with the first option because the resonances remained unshifted upon addition of additional Ni. Combining the spectral results allows us to suggest that both Ni are bound by N/O donors in five- or six-coordinate sites, but the first site is associated with more histidines than the second, which must possess at least two (from NMR and XAS data).

Table 3 Curve-fitting results for Cu EXAFS of H144* UreE[a]

Sample	Fit	Group	Shell	N_s	R_{as} (Å)	σ^2_{as} (Å^2)	ΔE_0 (eV)	f'	BVS
Truncated UrE	1	N/O	Cu-N	(2)	2.02	0.0045	2.70	0.070	2.04
1 Cu/dimer		imid	Cu-N_1	(2)	1.98	0.0024	[2.70]	<0.049>	
$k = 2.0$–12.0 Å^{-1}		imid	Cu-C_2	(2)	[2.97]	[0.0037]	[2.70]		
		imid	Cu-N_3	(2)	[4.11]	[0.0051]	[2.70]		
		imid	Cu-C_4	(2)	[4.14]	[0.0052]	[2.70]		
		imid	Cu-C_5	(2)	[3.01]	[0.0037]	[2.70]		
	2	N/O	Cu-N	(1)	2.04	0.0002[b]	0.57	0.074	2.12
		imid	Cu-N_1	(3)	1.97	0.0037	[0.57]	<0.056>	
		imid	Cu-C_2	(3)	[2.95]	[0.0056]	[0.57]		
		imid	Cu-N_3	(3)	[4.09]	[0.0078]	[0.57]		
		imid	Cu-X_4	(3)	[4.12]	[0.0078]	[0.57]		
		imid	Cu-C_5	(3)	[2.99]	[0.0057]	[0.57]		
	3	S	Cu-S	(0.5)	2.20	0.0049	1.64	0.063	2.16
		N/O	Cu-N	(1.5)	2.01	0.0058	[1.64]	<0.039>	
		imid	Cu-N_1	(2)	1.98	0.0022	[1.64]		
		imid	Cu-C_2	(2)	[2.96]	[0.0033]	[1.64]		
		imid	Cu-N_3	(2)	[4.11]	[0.0046]	[1.64]		
		imid	Cu-C_4	(2)	[4.13]	[0.0047]	[1.64]		
		imid	Cu-C_5	(2)	[3.00]	[0.0034]	[1.64]		
Truncated UreE	4	N/O	Cu-N	(2)	2.02	0.0049	2.57	0.070	2.04
2 Cu/dimer		imid	Cu-N_1	(2)	1.98	0.0032	[2.57]	<0.053>	
$k = 2.0 - 12.0$ Å^{-1}		imid	Cu-C_2	(2)	[2.97]	[0.0048]	[2.57]		
		imid	Cu-N_3	(2)	[4.12]	[0.0067]	[2.57]		
		imid	CuC_4	(2)	[4.14]	[0.0068]	[2.57]		
		imid	CuC_5	(2)	[3.01]	[0.0049]	[2.57]		
	5	N/O	Cu.N	(1)	2.05	0.0016	0.92	0.073	2.11
		imid	Cu-N_1	(3)	1.97	0.0039	[0.92]	<0.059>	
		imid	Cu-C_2	(3)	[2.96]	[0.0059]	[0.92]		
		imid	Cu-N_3	(3)	[4.10]	[0.0081]	[0.92]		
		imid	Cu-C_4	(3)	[4.13]	[0.0082]	[0.92]		
		imid	Cu-C_5	(3)	[3.00]	[0.0059]	[0.92]		
	6	S	Cu-S	(0.5)	2.24	0.0023	1.25	0.057	2.18
		N/O	Cu-N	(1.5)	2.00	0.0039	[1.25]	<0.038>	
		imid	Cu-N_1	(2)	1.97	0.0028	[1.25]		
		imid	Cu-C_2	(2)	[2.95]	[0.0042]	[1.25]		
		imid	Cu-N_3	(2)	[4.10]	[0.0058]	[1.25]		
		imid	Cu-C_4	(2)	[4.12]	[0.0058]	[1.25]		
		imid	Cu-C_5	(2)	[2.99]	[0.0042]	[1.25]		

[a] See footnotes to Table 2
[b] Underlined value is chemically or theoretically unreasonable

Cu binding to H144*UreE

The properties of Cu(II) bound to H144*UreE were examined by electronic, RR, EPR, and ESEEM spectroscopies as well as by XAS. For protein samples containing variable amounts of Cu, the intensites of the 370-nm feature in the electronic spectra suggest the presence of some cooperativity in Cu binding, with the charge-transfer transition arising from the protein with two Cu ions bound [9] (the 1Cu/dimer form is estimated to possess ~25% of the protein with 2Cu bound and ~50% of the protein with 1Cu bound). This band was abolished when the protein was subjected to cysteine modification by iodoacetamide, consistent with the presence of thiolate coordination in the untreated sample, while the d-d transition at 625 nm remains. The 2Cu/H144*UreE visible spectrum is nearly identical to that obtained when a single histidine ligand of Cu in CuZn-superoxide dismutase is substituted with a cysteine [23]. The 380-nm band in the modified superoxide dismutase has been assigned as a thiolate-to-Cu charge-transfer transition by comparison to other Cu-cysteine proteins. The higher energy of the Cu-H144*UreE-derived band is likely due to the presence of a strongly bound ligand directly *trans* to the sulfur donor [35]. The assignment of the electronic bands generated in the 2Cu/dimer sample as cysteine-to-Cu charge-transfer transitions is supported by the results of RR, which directly probes the Cu-S(cys) bond and shows several low frequency peaks. It is likely that several vibration modes, including the Cu-S stretching vibration, contribute to these bands [36]. The most intense peak centered at 315 cm^{-1} is typical of type 2 Cu-cysteine sites, and with the application of Badger's rule (as described in [37]), this number then gives an estimate of the Cu-S bond length as approximately 2.26 Å. The Cu(II) EPR data clearly show that the initial signal (g values of 2.28 and 2.06) in the 1Cu/dimer sample is retained in the

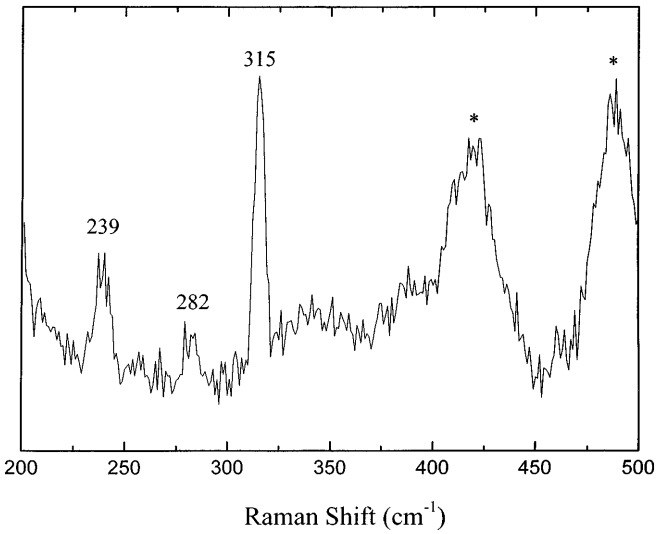

Fig. 7 RR spectrum (low-frequency region) of the 2Cu/dimer form of H144*UreE. Protein (0.45 mM dimer) was prepared in 10 mM HEPES buffer (pH 7.5), 0.9 mM $CuCl_2$, and 30% glycerol. The spectrum was obtained at 4 °C using 413.1 nm excitation at 13.5 mW. An average of 14 scans is shown. Peaks at 239, 282, and 315 cm^{-1} are due to Cu-H144*UreE, whereas those marked with asterisks are due to glycerol

2Cu/dimer sample, while a second signal (*g* values of 2.32 and 2.07) is superimposed on this feature. As in the case for Ni, the two Cu ions are bound in distinct sites. The ESEEM analyses indicate the presence of more than one equatorial histidine in each of the Cu coordination spheres. EXAFS fits support the presence of two histidines per Cu and are consistent with a Cu-S interaction at approximately 2.24 Å, apparent in the 2Cu/dimer sample. Combining the spectral results allows us to suggest that the first Cu is bound in a tetragonal site including two histidine ligands, whereas the second Cu is bound in a tetragonal site including two histidine and one cysteine. The overall coordination appears to be 4 according to EXAFS fits, but is most likely to be 5 according to the EPR and optical spectra. Weak axial ligation would not be detected by EXAFS. The presence of a cysteine donor for the second Cu center contrasts with Ni binding exclusively by N/O ligands for both of its sites in this protein.

Co binding to H144*UreE

The binding of Co(II) by H144*UreE was examined by electronic and NMR spectroscopies. The visible spectra obtained for the 1 and 2Co/dimer samples suggest pseudo-octahedral geometry and the absence of a charge-transfer transition; hence the site appears to lack the cysteine donor observed for Cu. The proton NMR spectra show evidence for sequential binding of the two metal ions and indicate a total of three observable histidine donors to Co. Unlike the case for the Ni binding sites, however, the order of binding is reversed, with two histidines observed at the first binding site and one in the second. Paramagnetically shifted peaks located at approximately 15 ppm may be due to the methylene proteins of other amino acids which serve as ligands to the Co(II) ion.

Implications for urease assembly

In vivo synthesis of urease requires the selective incorporation of Ni into urease apoenzyme by a process that has been proposed to use UreE as a Ni shuttle or metallochaperone [8]. Some metal ion specificity in this process is clearly conferred by UreE or H144*UreE, because Ni binding to the accessory protein exhibits no competition with the biologically significant metal ions Mg, Mn, and Ca [8, 9]. On the other hand, selected divalent metal ions do compete for the two Ni sites on the homodimer. For example, when using 10 μM $NiCl_2$ (where H144*UreE is approximately half saturated) the amount of bound Ni is further reduced by 50% in the presence of ~10 μM Cu, ~40 μM Zn, ~100 μM Co, and ~400 μM Cd [9]. As described above, our spectroscopic studies of the Ni-, Cu-, and Co-bound forms of H144*UreE suggest that the coordination environments of these metal ions are distinct. This result raises the possibility that only the Ni-bound form of H144*UreE possesses the appropriate conformation to interact with urease apoprotein; i.e., Cu and Co ions can bind to H144*UreE, but the distinct coordination environments imposed by these metals (e.g. including a thiolate ligand in the case of the 2Cu/dimer protein) lead to protein conformations that are non-productive for urease apoprotein interaction. Thus, we propose that UreE functions specifically in Ni delivery to urease despite its ability to bind other metal ions. Given that urease possesses a dinuclear metallocenter, it is interesting to note that the functionally active H144*UreE binds 2Ni/dimer. We speculate that the dimer simultaneously delivers both of its bound Ni ions during activation of a single urease active site.

Acknowledgements This work was supported by the National Institutes of Health (DK 45686 to R.P.H.; GM 54065 and S10-RR10381 to J.M.; GM 25480 to G.T.B.; and GM 42025 to R.A.S.) and the Human Frontiers Program (to G.T.B.). The XAS data were collected at the Stanford Synchrotron Radiation Laboratory (SSRL), which is operated by the Department of Energy, Division of Chemical Sciences. The SSRL Biotechnology Program is supported by the N. I. H., Biomedical Resource Technology Program, Division of Research Resources.

References

1. Mobley HLT, Island MD, Hausinger RP (1995) Microbiol Rev 59:451–480
2. Jabri E, Carr MB, Hausinger RP, Karplus PA (1995) Science 268:998–1004
3. Lee MH, Mulrooney SB, Renner MJ, Markowicz Y, Hausinger RP (1992) J Bacteriol 174:4324–4330

4. Moncrief MBC, Hausinger RP (1996) In: Hausinger RP, Eichhorn GL, Marzilli LG (eds) Mechanisms of metallocenter assembly. VCH, New York, pp 151–171
5. Park I-S, Carr MB, Hausinger RP (1994) Proc Nat Acad Sci USA 91:3233–3237
6. Moncrief MBC, Hausinger RP (1996) J Bacteriol 178:5417–5421
7. Park I-S, Hausinger RP (1995) J Bacteriol 177:1947–1951
8. Lee MH, Pankratz HS, Wang S, Scott RA, Finnegan MG, Johnson MK, Ippolito JA, Christianson DW, Hausinger RP (1993) Protein Sci 2:1042–1052
9. Brayman TG, Hausinger RP (1996) J Bacteriol 178:5410–5416
10. McCracken J, Shin D-H, Dye JL (1992) Appl Mag Res 3:305–316
11. Mims W (1984) J Mag Res 59:291–306
12. Hore PJ (1983) J Mag Res 55:283–300
13. Scott RA (1985) Meth Enzymol 117:414–459
14. Fransson G, Lundberg BKS (1972) Acta Chem Scand 26:3969–3976
15. Konopelski JP, Reimann CW, Hubbard CR, Mighell AD, Santoro A (1976) Acta Cryst, Sect B 32:2911–2913
16. Rehr JJ, Albers RC (1990) Physical Rev B 41:8139–8149
17. Mustre de Leon J, Rehr JJ, Zabinsky SI, Albers RC (1990) Physical Rev B 44:4146–4156
18. Rehr JJ, Mustre de Leon J, Zabinsky SI, Albers RC (1991) J Am Chem Soc 113:5135–5140
19. Brown ID, Altermatt D (1985) Acta Cryst 1341:244–247
20. Thorp HH (1992) Inorg Chem 31:1585–1588
21. Liu W, Thorp HH (1993) Inorg Chem 32:4102–4105
22. Ming L-J, Que L Jr, Kriauciunas A, Frolik CA, Chen VJ (1990) Inorg Chem 29:1111–1112
23. Lu Y, Gralla EB, Roe JA, Valentine JS (1992) J Am Chem Soc 114:3560–3562
24. Cotton FA, Wilkenson G (1980) Advanced inorganic chemistry. Wiley, New York
25. Rotilio G, Agro AF, Calabrese L, Bossa F, Guerrieri P, Mondovi B (1971) Biochem 10:616–621
26. Mims WB, Peisach J (1978) J Chem Phys 69:4921–4930
27. Lin CP, Bowman MK, Norris JR (1994) J Chem Phys 85:56–62
28. Kosman DJ, Peisach J, Mims WB (1980) Biochem 19:1304–1308
29. McCracken J, Pember S, Benkovic SJ, Villafranca JJ, Miller RJ, Peisach J (1988) J Am Chem Soc 110:1069–1074
30. Jiang F, McCracken J, Peisach J (1990) J Am Chem Soc 112:9035–9044
31. Colpas GJ, Maroney MJ, Bagyinka C, Kumar M, Willis WS, Suib SL, Baidya N, Mascharak PK (1991) Inorg Chem 30:920–928
32. Bertini I, Borghi E, Luchinat C, Monnanni R (1982) Inorg Chem Acta 67:99–102
33. Rosenberg RC, Root CA, Gray HB (1975) J Am Chem Soc 97:21–26
34. Ming L-J, Valentine JS (1990) J Am Chem Soc 112:6374–6383
35. Andrew CR, Sanders-Loehr J (1996) Acc Chem Res 29:365–372
36. Andrew CR, Han J, Blaauwen T den, Pouderoyen G van, Vijgenboom E, Canters GW, Loehr TM, Sanders-Loehr J (1997) JBIC 2:98–107
37. Andrew CR, Yeom H, Valentine JS, Karlsson BG, Bonander N, Pouderoyen G van, Canters GW, Loehr TM, Sanders-Loehr J (1994) J Am Chem Soc 116:11489–11498